E-beam Fluorinated CVD Graphene: in-situ XPS study on stability and NH3 adsorption doping effect

Vincent Malesys, Tianbo Duan, Emmanuel Denys, Hu Li, Klaus Leifer, Laurent Simon

E-beam Fluorinated CVD Graphene: in-situ XPS study on stability and NH_3 adsorption doping effect

V. Malesys[1*], T. Duan[2], E. Denys[1], Hu Li[2,3], K. Leifer[2], L. Simon[1]
[1]Institut de Sciences des Matériaux de Mulhouse, CNRS-UMR 7361, Université de Haute Alsace, Mulhouse, France
[2]Department of Engineering Sciences, Ångström Laboratory, Uppsala University, 75121 Uppsala, Sweden
[3]Shandong Technology Centre of Nanodevices and Integration, School of Microelectronics, Shandong University, Jinan 250101, China

Email: vincent.malesys@uha.fr

Received xxxxxx
Accepted for publication xxxxxx
Published xxxxxx

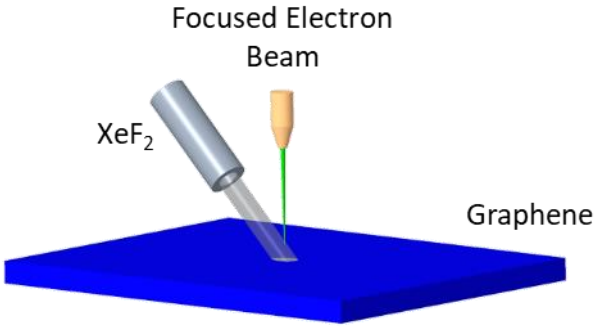

Figure 1. Scheme illustrating the process of graphene fluorination via electronic irradiation and the introduction of gaseous XeF_2. Unlike scenarios involving the creation of carbon radicals, this method relies on the presence of fluorine radicals to facilitate the formation of bonds between carbon and fluorine atoms.

Abstract

Graphene exhibits promise in gas detection applications despite its limited selectivity. Functionalization with fluorine atoms offers a potential solution to enhance selectivity, particularly towards ammonia (NH+) molecules. This article presents a study on electron-beam fluorinated graphene (FG) and its integration into gas sensor platforms. We begin by characterizing the thermal stability of fluorographene, demonstrating its resilience up to 450°C. Subsequently, we investigate the nature of NH_3 interaction with FG, exploring distinct adsorption energies to address preferential adsorption concerns. Notably, we introduce an innovative approach utilizing XPS cartography for simultaneous analysis of fluorinated and pristine graphene, offering enhanced insights into their properties and interactions. This study contributes to advancing the understanding and application of fluorinated graphene in gas sensing technologies.

Keywords: Fluorographene, XPS mapping, gas detection, ammonia reactivity, thermal stability.

1. Introduction

The reinforcement of environmental and health standards reveals the need for better air quality monitoring involving the control of nitrogen dioxide (NO_2) and ammonia (NH_3) emissions [1–3]. For this, it is necessary to be able to follow the concentration of these toxic gases in the environment, at the exit of a catalytic converter or within a dwelling with sensors having sensitivities to the part per billion (ppb) for the gases of interest, and insensitivity to moisture and even more to other potentially present gases (CO, SO_2, H_2, Ethylene, Cl_2, etc.). According to WHO estimates, about seven million premature deaths worldwide each year are due to the combined effects of outdoor and indoor air pollution [4,5]. For example, the annual reference threshold for NO_2 exposure is 10 µg/m^3 or 5 ppb. In this context, two-dimensional materials, such as novel 2D transition metal dichalcogenides (TMDs) [6] and even more graphene, consisting of only a few atomic carbon planes and with an increased sensitivity to the environment suggest a technological revolution for the detection of toxic gases [7–12].

One of the limitations of these devices is related to the very nature of graphene and concerns the selectivity of gas sensors. Indeed, graphene is particularly sensitive to ammonia and nitrogen dioxide, but it is also reactive with many species present in the atmosphere [7,10,13]. This limits the possible applications of our sensors. Numerous studies have focused on graphene functionalisation by different methods [14] to overcome the disadvantage of the limited selectivity that reduces its potential applications. Creating a graphene sensor with specific chemical selectivity can be achieved through functionalization, which involves locally modifying the graphene layer to alter its affinity, doping characteristics or band properties [15].

There is a very strong electronic affinity between fluorine, F, and the NH_3 molecule [16–18]. Indeed, fluorine is the most electronegative element, thus it has strong interactions with other functional groups or molecules, which is favourable for gas detection applications, especially for NH_3 [19]. There are numerous techniques for functionalizing graphene with fluorine [20]. There are mainly two pathways for the synthesis of fluorographene: one involves starting from graphite fluoride [21–23], which allows direct production of fluorographene through mechanical exfoliation or liquid-phase exfoliation of the crystal, and the other involves fluorination after the synthesis of graphene by CVD or exfoliation [17,24–27]. The choice of fluorination technique is made based on the available graphene sources following the existing functionalization methods. This strongly influences the final properties of fluorographene: crystallinity, arrangements within the graphene lattice, nature of bonds, thermal and chemical stability, electrical characteristics, as well as interactions with other species. Finally, the technique used will define the quantities of fluoride added, the electronic and crystalline properties of graphene and it will also define the future applications of devices integrating fluorographene [28,22,29–34,21,35,27,36–39].

Although there are many examples of fluorographene devices, gas sensing remains a field promising field to explore. A first device was presented by Tadi et al. [16] in 2016 for the detection of NH_3 in the liquid phase. The developed sensor is manufactured from two sources of fluorinated graphene oxide: one with 5% atomic fluorine, and the other with 24%. The obtained fluorographene is stable up to 400°C. It is a sensor with large surfaces of fluorinated graphene (FG) onto which electrodes are deposited by lithography, to construct a detector using impedance spectroscopy. Their sensors exhibit a 30 s response time and the fluorinated graphene device has a sensitivity improved by a factor of 3 to NH_3 as compared to pristine graphene.

A second publication by Zhang et al. [40] presents a gas sensor based on CVD-grown and fluorinated, in a reactive ion etching system with a SF_6 plasma, graphene for NH_3 detection. The sensor is a chemo-resistive device with a layer of fluorographene on SiO_2/Si and contacted by Au/Ti electrodes. The fluorinated graphene-based gas sensor exhibits a rapid response and recovery time of a few tens of seconds. Its response is repeatable, and the regeneration phase allows for complete sensor restoration. The sensitivity, better than that of the pristine graphene sensor, enables the detection of 2 ppm of ammonia at room temperature.

Similar results were reported by Kang et al. [41]. They developped a chemosensitive sensor using exfoliated oxidised graphene fluoride that is 3.5 times more sensitive than its pristine graphene homologue. Kim et al. [19] built a chemically fluorinated graphene oxide device with a 20 times enhanced response compared to their reduced graphene oxide reference sensor. They attributed their result to the modification in charge distribution across the functional groups, leading to changes in gas adsorption energies. Equally, Duan et al. [42] demonstrated that their site-selective ion-beam-induced fluorinated graphene sensor has a 8 times better sensitivity with compared to their counterparts device based on pristine graphene.

Most of these studies focused on the fluorination of graphene with defects, graphene oxide (GO), and reduced graphene oxide (rGO), or functionalized graphene with holes, where fluorine atoms decorate the defects. To the best of our knowledge, none of them address fluorinated pristine graphene without intentional or unintentional defects.

In order to use fluorination for a gas sensor application, certain criteria must be met. Firstly, fluorination must be stable over time, i.e., the graphene must remain fluorinated even after several months. Similarly, fluorination must be thermally stable at over 200°C to allow for sensor reset by annealing without desorbing the fluorine [28]. It has been proven that fluorographene produced through the exfoliation

method exhibited exceptionally high thermal stability, even after being heated above 450°C [22,25]. Fluorographene with a reduced fluorine content seems to undergo a defluorination process when exposed to high temperatures [28,43,44]. Since stability is highly dependent on the synthesis process and the structure of fluorographene, this becomes a crucial aspect to study when exploring a new fluorination technique, such as e-beam functionalization.

Following our previous work on the development of a graphene gas sensor [45] we present here a fluorination of pristine graphene which can be localized spatially on the final device on graphene segments, at the end of fabrication and compatible with the whole process of sensor fabrication. Indeed this process is 'clean' and does not harm the sensor. It excludes liquid-phase fluorination processes [46] that could introduce contaminations or damage the sensor.

Recently some of us have developed a new method of fluorination which can be done after the realization of the device without degradation. In this article, building upon preliminary research conducted at Uppsala University on electron-beam fluorination [47], as well as broader investigations into graphene fluorination [18,48] and fluorinated graphene gas sensors [42], we present a novel X-ray photoelectron spectroscopy (XPS) study of e-fluorinated graphene, focusing on elucidating the adsorption and desorption behaviour of NH_3 on the graphene. Our primary objectives include characterizing the material's stability over time and at different temperatures, crucial parameters for its application as a resettable gas sensor. Additionally, we delve into the interactions and adsorption/desorption mechanisms of NH_3 on the surface of fluorographene. To achieve this, we propose an original approach utilizing XPS mapping to simultaneously visualize both pristine and fluorinated graphene—an innovative technique with limited precedent in the literature [49–51].

2. Materials and Methods

Local fluorination of graphene is performed using electron-beam activation within a FEI Strata DB235 FIB/SEM operating at 10^{-6} mbar, employing an electron acceleration voltage of 5 kV and a beam current of 650 pA. XeF_2 molecules are introduced via a gas injection system (GIS) within the FIB/SEM chamber, with a partial pressure at the gas nozzle exit set at 600 Pa. The fluorination process occurs concurrently with electron beam irradiation and XeF_2 molecule injection.

Commercially obtained chemical vapour-deposited (CVD) graphene on a Cu foil (monolayer, Graphenea, San Sebastián, Spain) serves as the primary material. Graphene transfer to a Si substrate covered with 300 nm thick SiO_2 is facilitated through a PMMA-assisted transfer process [52]. Subsequently, graphene channels and electrical contacts are fabricated utilizing electron beam lithography (NanoBeam nB5, NBL, London, United Kingdom) and low-power O_2 plasma etching (Vision 320 RIE, Advanced Vacuum, Bernin, France), followed by a metal evaporation/lift-off process involving Ti (5 nm)/Au (50 nm).

Photoelectron spectroscopy (XPS) measurements were performed in situ using a VG Scienta R3000 spectrometer equipped with a hemispherical analyzer. An energy resolution of 16 meV is reached with a pass energy of 20 eV. We used a monochromatic X-ray source (AlKα, 1486.6 eV). The protocol for analysis involved examining both pristine graphene and fluorinated graphene within and outside designated marking zones described in the next paragraph. To achieve spatial resolution, instead of one channel in the integrated mode, we divide the output detector of the analyzer by 115 channels to ensure a sufficient signal-to-noise ratio. The analysis was performed in "XPS imaging" mode, where mappings were generated according to an intensity scale. These mappings depicted binding energy of the core level peak on the x-axis and window position in millimetres on the y-axis, providing valuable insights into the material composition and distribution.

In order to conduct X-ray photoelectron spectroscopy (XPS) studies using our XPS setup, we devised an innovative approach in collaboration with Uppsala University. Samples need to possess a sufficiently large surface area, at least 100 µm² on a 1 cm² substrate, to ensure adequate signal acquisition during analyses. However, electron fluorination incurs significant time and monetary costs. Moreover, we aimed to investigate both pristine and fluorinated graphene on the same sample. Consequently, we opted to mark 300 x 300 µm surfaces with a 100 µm gold square deposited via evaporation and electron lithography. Within these gold squares, graphene underwent fluorination, while remaining pristine elsewhere. This marking facilitated precise localization of the fluorinated area during analysis, leveraging the distinctive gold signal for easy determination of the analysis region. Additionally, the marking helped mitigate charging effects induced by XPS. A schematic representation of the constructed samples can be found in Figure 2.

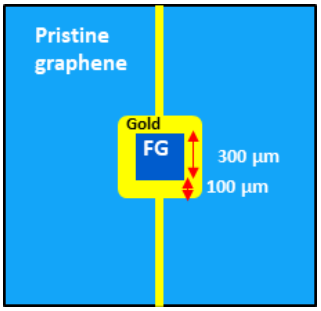

Figure 2. Scheme of a fluorinated graphene sample with identification of the pristine graphene area, the gold reference square, the fluorinated area (FG) as well as conductive wires connecting the gold square electrically to the border of the sample.

Initially, it is essential to evaluate the impact of fluorination on our samples and compare the resulting fluorographene with the pristine graphene also present on the device. We pinpoint the fluorinated graphene region using both the Au4f core level and the F1s signal. In Figure 3, we illustrate two typical spectra corresponding to graphene and fluorinated graphene. For pristine, non-fluorinated graphene **(**Figure 3 (a)), only the characteristic sp^2 and sp^3 components are evident, respectively around 284−285 and 285−286 eV. Conversely, the characterization of fluorinated graphene (Figure 3 (b)) reveals not only the typical sp^2 and sp^3 components of graphene. Additionally, two distinct components indicative of fluorine-carbon bonds were observed: the first around 287−288 eV (referred to as CF1 in this article) and the second near 290−291 eV (CF2). The CF1 component could be attributed to semi-ionic C−F bonds, while the CF2 component may correspond to covalent C−F [20,24,43,53–59].

In fact, these components cannot be attributed to those two types: a covalent C-F bond and a semi-ionic C-F bond. Instead, they are more likely associated with C-F and C-F2 bonds at defect sites. A semi-ionic C-F bond would give rise to a second component in the F1s core-level peak, shifted by 1.8 eV toward lower binding energy, as reported by A. Tressaud *et al*. [60]. However, this shift is not observed here.

Indeed, although the weak intensity of the peaks limits our ability to draw strong conclusions, the F1s core-level peaks appear symmetrical. This observation challenges the hypothesis of distinct iono-covalent and covalent bonds, instead supporting the interpretation that the peaks predominantly correspond to C-F and C-F2 bonds at defect sites, as previously observed by some of us using the same technology [47] or with a chemical approach [22].

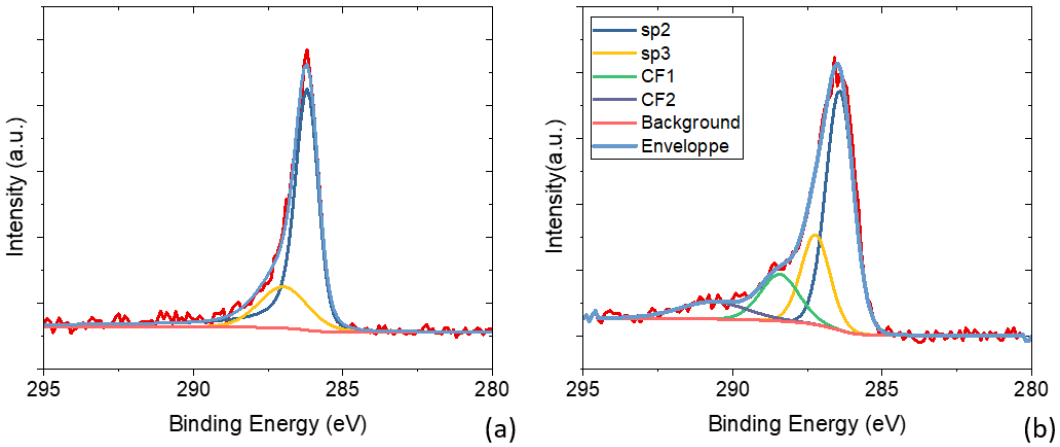

Figure 3. XPS spectra of the C1s extracted from the pristine area in (a) and from the fluorinated area in (b).

In summary, electron-beam fluorination offers the capability to functionalize graphene with nanoscale precision and precise regulation of fluorine content, resulting in the formation of CxF structures. Unlike more cumbersome chemical methods or functionalization strategies reliant on inducing defects, this technique avoids introducing defects into the graphene lattice. It enables fluorination of the sensor post-manufacture with exact fluorine levels. Additionally, it offers the advantage of selective application to specific graphene regions on a sensor.

Finally, we would like to point out that the functionalization of graphene sheets could damage it. Indeed, the gaseous XeF_2 is also used for the etching of silicon, phenomenon enhanced in the presence of an external source of energy (here electron beam). To assess the morphological integrity of the surface, we have performed AFM analysis on the pristine area (Figure 4 (a)) and on the fluorinated area (Figure 4 (b)). The roughness was measured, they are ranging between 0.39 ± 0,03 and 0.46 ± 0,04 nm for fluorinated and pristine graphene, respectively allowing to conclude that our electronic fluorination process does not cause morphological degradation of graphene.

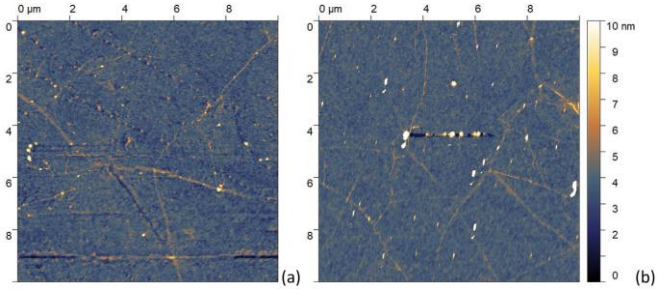

Figure 4. AFM imaging of GFluore samples based on the scanned area, with (a) non-fluorinated graphene and (b) fluorinated graphene.

3. Temperature stability of the e-fluorinated Graphene

In the context of utilizing fluorographene in a graphene-based gas sensor, it is crucial to demonstrate its resilience to repeated high-temperature annealing cycles while maintaining stability over time. The ability to desorb captured gas for

sensor reusability hinges on heating the material to the highest possible temperature without compromising functionality, with 450°C identified as the upper limit to prevent degradation of the detector and lithographed contacts. The established protocol for this investigation is straightforward. Initially, it involves characterizing the sample pre-annealing, focusing on the C1s and F1s core level peaks in fluorinated and non-fluorinated areas to define the initial state of fluorographene and discern peak components and their relative areas. Throughout the analysis and after each step, systematic imaging of Au4f core levels is conducted to confirm the overall robustness of the device. These spectral analyses are complemented by mapping analyses to observe the size and position of different discernible zones, notably the fluorinated zone and the gold reference square. Subsequently, the sample undergoes transfer under vacuum to another chamber for annealing before returning for XPS analysis. The same analyses conducted initially are performed on C1s, F1s, and Au4f. This process is repeated with annealing temperatures varying from 100°C to 450°C.

We conducted mappings of the Au4f: pristine and after annealing at 450°C (Figure 5). No discernible differences were observed between the two, indicating the thermal stability of the gold square. This observation corroborates the robustness of the fluorinated 2D material against thermal degradation, which is crucial for maintaining the integrity and functionality of the device over time.

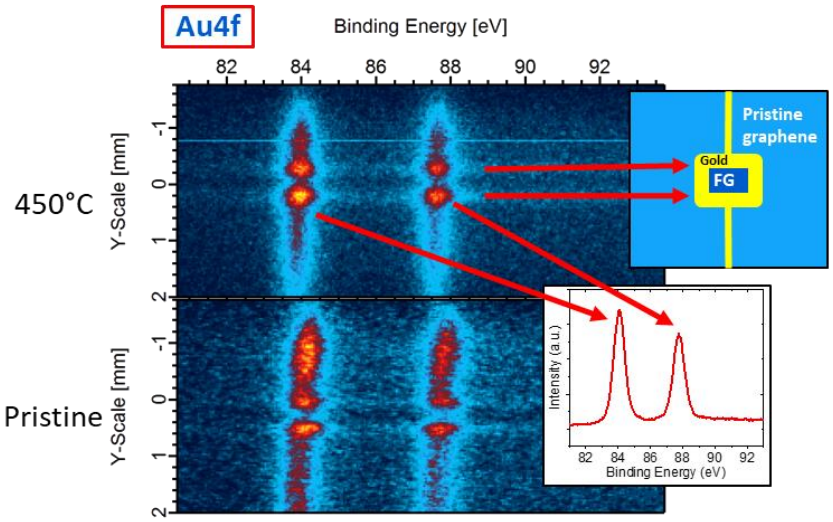

Figure 5. XPS mapping of Au4f before and after annealing at 450°C. On the right is inserted the scheme of the device with the gold square to show the corresponding higher signal on the Y axis (position). At the bottom right is present the XPS spectra of the Au4f, with the Au4f 7/2 and the Au4F 5/2 peaks respectively at 84 and 88 eV, to highlight the two bands visible on the X axis (binding energy).

Following annealing at temperatures of 100°C, 250°C, and 450°C, we analysed both the C1s and F1s (Figure 6) mappings. Surprisingly, there was no noticeable alteration in the intensity of the C1s peak across the entire analysis range encompassing both fluorinated and non-fluorinated regions. This consistent intensity underscores the stability of both graphene and fluorinated graphene, as they demonstrate no desorption tendencies under the influence of annealing. Additionally, the F1s peak, precisely located within the fluorinated square, exhibited consistent intensity, further confirming the stability of fluorinated graphene. Interestingly, a shift towards lower binding energies in the C1s and F1s position was observed following the initial annealing at 100°C. This - 1.5 eV shift reveals the doping induced by the presence and then the absence of hydroxyl groups on the analysed surface [61].

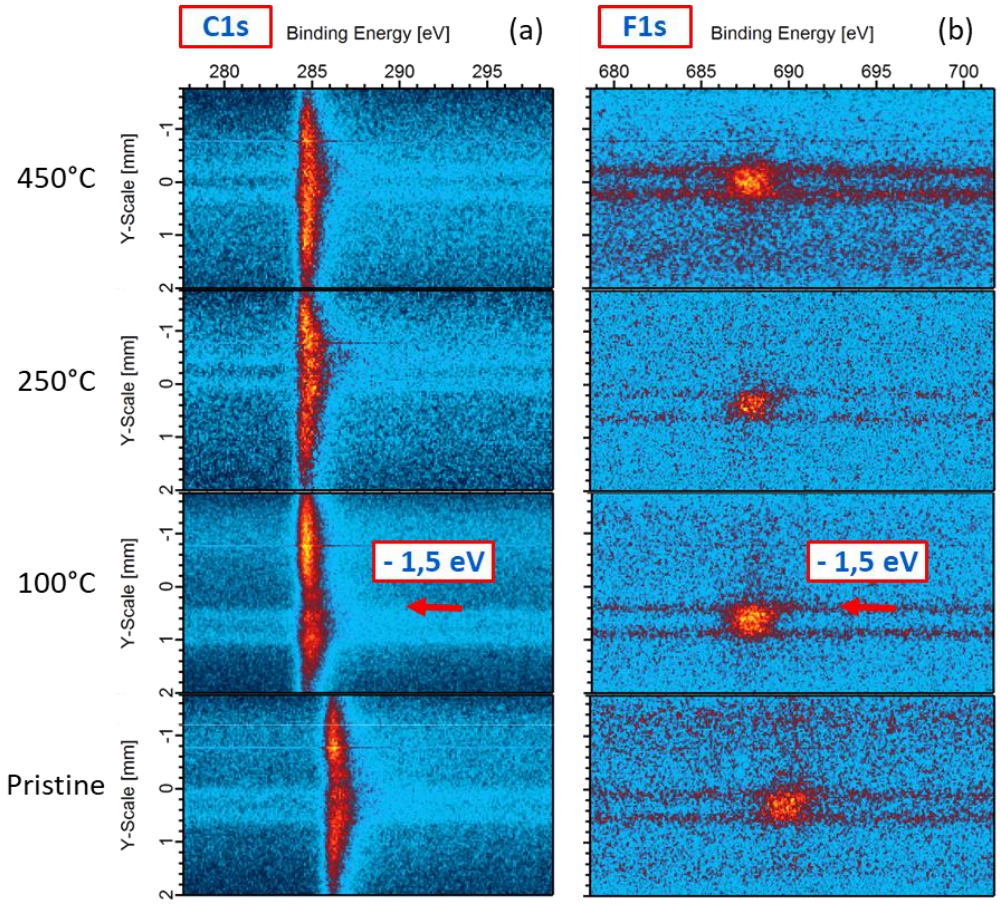

Figure 6. XPS mappings of (a) C1s and (b) N1s before annealing and after annealing at 100°C, 250°C, and 450°C of the fluorinated graphene sample.

To validate the mapping characterisation, we examined both the C1s and F1s spectra within the fluorinated region (depicted in Figure 7), selecting appropriate channels for analysis. Similarly, no discernible differences were observed in peak intensities. Thus the -1.5 eV shift in both C1s and F1s positions is also present. Notably, except a slight decrease of the CF2 component intensity no changes were observed in the sp^2, sp^3, CF1, and CF2 components of the C1s spectra. The proportions of the different components remain stable during annealing. We did not observe any changes in the hybridizations of graphene and the bonds between graphene and fluorine atoms. Thus, also from the analysis of the spectra, we conclude that the fluorographene remains stable up to 450°C assessing the thermal stability of the fluorinated graphene.

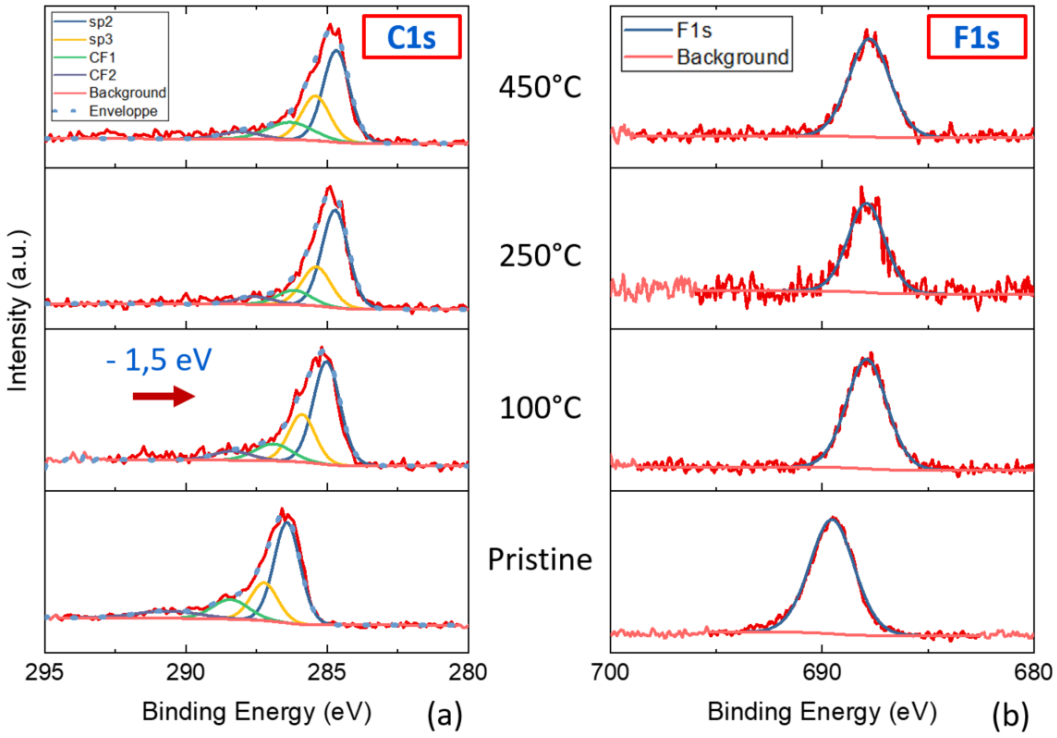

Figure 7. XPS spectra of (a) C1s and (b) N1s before and after annealing at 100°C, 250°C, and 450°C of the fluorinated graphene.

As a reference, the same analysis of the C1s in the non-fluorinated graphene zone was performed and is presented in Figure 8. It shows no modification of the sp^2 and sp^3 components following annealing up to 450°C. This is an expected result, as graphene has already demonstrated its temperature stability [62,63].

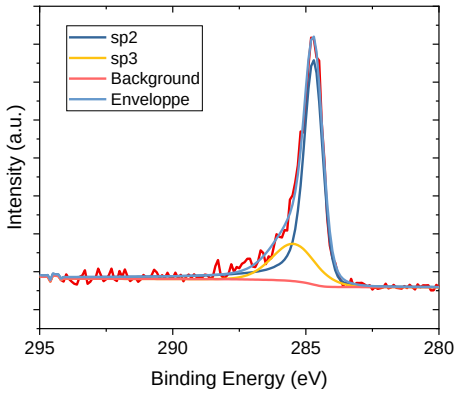

Figure 8. XPS spectrum of C1s from the non-fluorinated zone after annealing at 450°C.

This study highlights the resilience and stability of the e-beam fluorographene as a prelude for gas sensing application, through an analysis of the NH_3 adsorption. It emphases g its robustness and thermal stability under harsh conditions. Through systematic analysis, we demonstrated its structural integrity and functionality, even after repeated high-temperature annealing cycles, with 450°C as the upper limit. Analysis of C1s and F1s mappings and spectra revealed consistent peak intensities. This is useful not only for the gas sensing application but also in the case of other applications which need a graphene structuration by fluoration.

4. Study of the adsorption and desorption of NH_3

We investigated the interactions between the ammonia molecule and graphene using XPS. This technique enables us to elucidate the doping and charging effects induced by the exposure of fluorinated graphene to gas. Following gas exposure and sample characterization, we conducted annealing at 250°C to assess the reversibility of the process. Additionally, an initial regeneration step is prompted by the ultra-high vacuum conditions of the experiment, leading to the gradual desorption of NH_3 over time. Depending on the gas concentrations injected into the dedicated exposure chamber in which samples are transferred in UHV in between the analysis, the samples were initially exposed to a few Langmuir of NH_3, ultimately reaching 10 mbar of ammonia, corresponding to a NH_3 concentration of several parts per million (ppm) of gas in the chamber. This study focuses on exposure of the e-fluorographene to a pressure of 10 mbar of NH_3.

Figure 9 (a) allows us to observe the C1s across the entire analysis window. Initially, the C1s is at 284.5 eV, its "pristine" position as observed previously. After exposure to NH_3, it is centered at 289.5 eV, then shifts towards 286.5 eV before the desorption annealing, indicating a first step of NH_3 molecule

desorption from the surface induced by the vacuum of the XPS analysis setup. Indeed, the sample remained for several hours under ultra-high vacuum before annealing and in this period, the C1s peak remains stable. Finally, it returns to its initial position at 284.5 eV after annealing at 250°C. The shift of the C1s peaks towards higher binding energies observed after exposure to NH_3 is indicative of n-type doping and it is non-specific to the fluorinated area. It is strongest immediately after exposure and returns to its initial, non-doped position with the action of pumping and (or) annealing.

An identical phenomenon is observed when monitoring the F1s in Figure 9 (b). F1s is initially centred at 687.5 eV, shifting to 692.5 eV post-NH_3 exposure, then to 690 eV under vacuum, then returning to 687.5 eV after annealing at 250°C, indicating reversible NH_3 desorption.

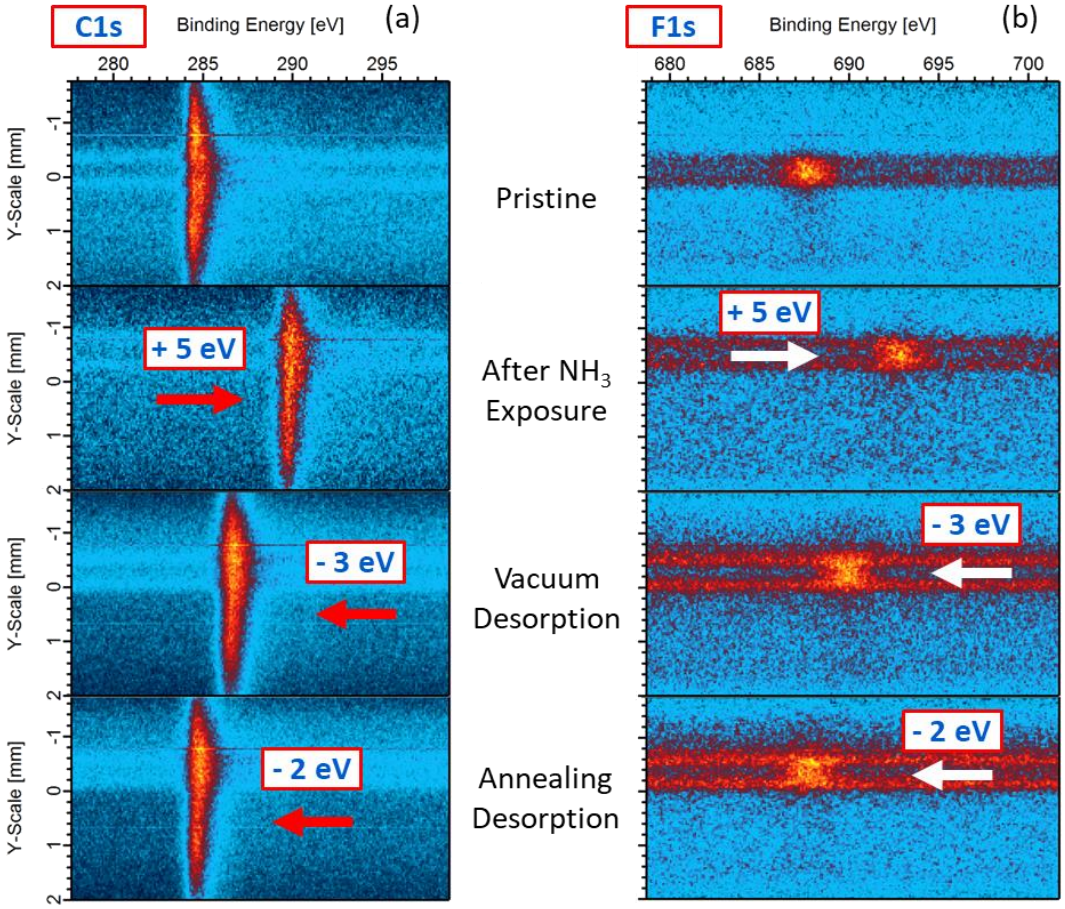

Figure 9. XPS mapping during exposure to NH_3 of the fluorinated graphene sample with the evolution of C1s in (a) and F1s in (b) before and after exposure to 10 mbar of NH_3, after vacuum desorption and after annealing at 250°C.

The monitoring of N1s mapping (Figure 10) and spectra (Figure 12) confirms the presence of NH_3 on the surface of the sample after the exposure and its distribution uniformly across its entity. The double band visible on the mapping (Figure 10) after exposure between 0 and -1 mm is caused by the remanence of Au4f peaks (background continuum rise due to inelastic electrons). The absence of a notable zone between 400 and 405 eV, the expected binding energies of N1s, indicates the lack of a preferential adsorption zone for ammonia on the sample surface. Indeed, the study of the spectra ((Figure 12) confirms this with the presence of the N1s peak visible on all channels of the window.

However, nitrogen is still visible after the regeneration process (either in mappings or spectra), demonstrating the final presence of NH_3. The N1s signal detected at the end of the process may be attributed to NH_3 molecules that lingered but did not interact with either fluorinated graphene (FG) or pristine graphene as it has been shown in Figure 9 that the doping effect on C1s and F1s is fully reversible.

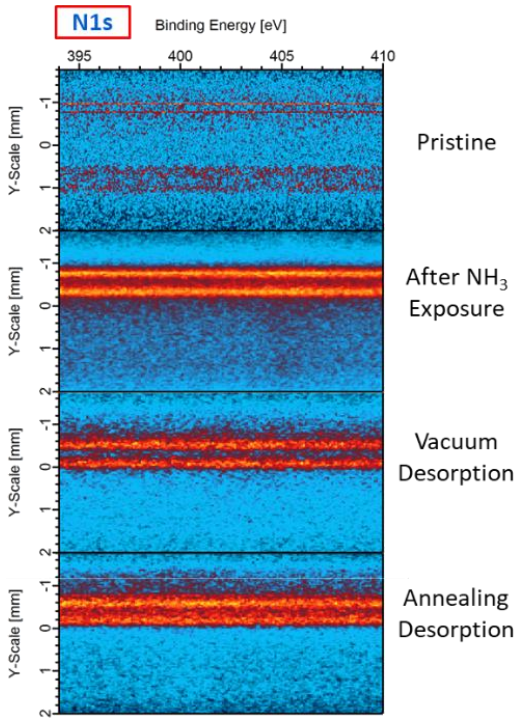

Figure 10. XPS mapping during exposure to NH_3 of the fluorinated graphene sample with the evolution of N1s before and after exposure to 10 mbar of NH_3, after vacuum desorption and after annealing at 250°C.

The comprehensive examination of spectra originating from the fluorinated, both pre and post-exposure to 10 mbar of NH_3, and pre and post-annealing at 250°C, is depicted in Figure 11 (a). Consistently, the spectra exhibit the same constituents as previously observed, including sp^2 and sp^3 of graphene, alongside CF1 and CF2 representing the carbon-fluorine bonds. Similar to the mappings, we observe consistent shifts in the C1s peaks: initially towards higher binding energies post-exposure, followed by a return to their initial positions post-pumping and annealing. Throughout this experiment, there is no discernible alteration in the shapes and intensities of the sp^2, sp^3, CF1, and CF2 components, suggesting that the integrity of the bonds within the fluorographene lattice remains unaffected by the adsorption and subsequent desorption of ammonia on the surface.

A similar investigation is conducted in the pristine region, illustrated in Figure 11 (b). The findings reveal identical reversible doping effects, along with no alteration in the sp^2 and sp^3 components.

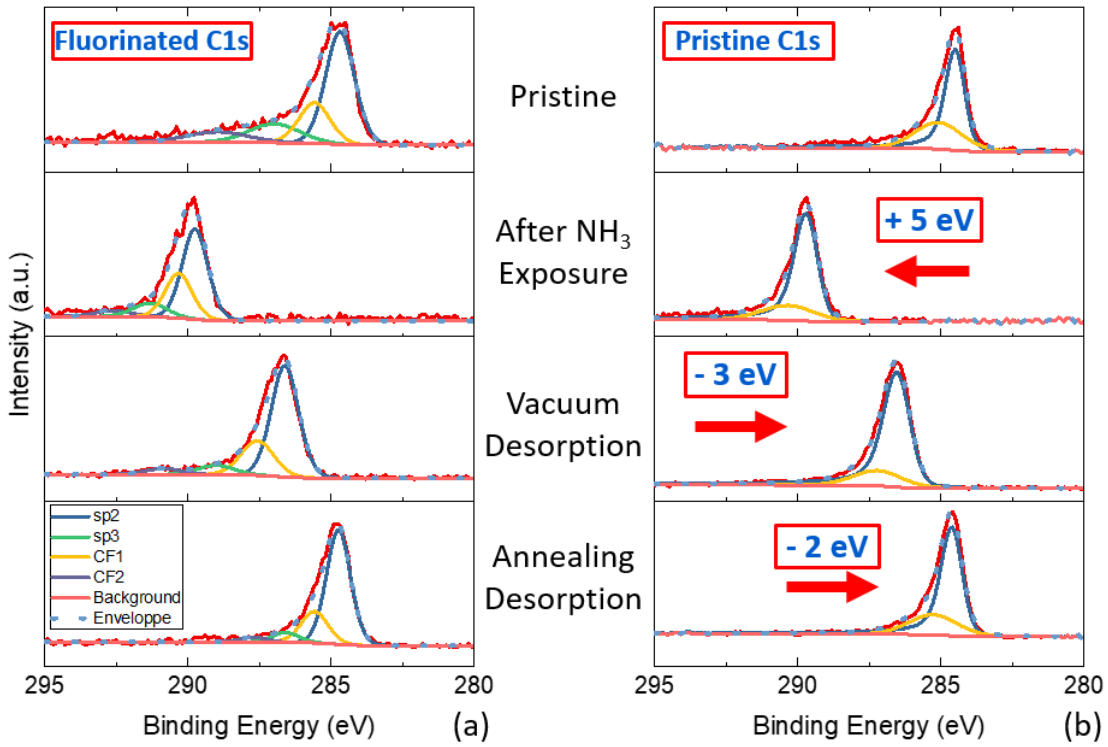

Figure 11. XPS spectra of the C1s from the fluorinated zone (a) and the pristine zone (b) before and after exposure to 10 mbar of NH_3, after a first step of vacuum desorption and after annealing at 250°C.

Similarly, the XPS spectra of N1s are examined in Figure 12 (a) before and after exposure to 10 mbar of NH_3, and before and after annealing at 250°C. These spectra exhibit consistent shifts towards higher binding energies, transitioning from

284.7 eV pre-exposure to 289.8 eV post-exposure, then from 286.6 eV to 284.7 eV following vacuum treatment and annealing. Notably, before exposure, there is no discernible N1s peak, as no nitrogen species were introduced into the chamber beforehand. Moreover, there is no disappearance of the N1s peak after annealing. The persistence of the nitrogen peak post-annealing at 250°C suggests the presence of residual NH_3 molecules on the sample surface, albeit without interaction with the fluorinated graphene, as indicated by the peak shifts back to their initial positions. It is likely that after a long exposure period, ammonia eventually adsorbs onto all surfaces within the chamber, Including diffusion into the substrate of our devices. Ammonia can notably adsorb beneath the graphene into the SiO_2 substrate, making it challenging to dislodge. This likely explains the difficulties in completely desorbing nitrogen from the samples, even after annealing at 250°C. On the other hand, the return of the C1s peaks and the sp^2, sp^3, CF1, and CF2 components to their initial positions before exposure indicates, at the very least, that NH_3 has been desorbed from the fluorinated graphene. The effects of charging and doping are nullified through annealing. As observed in Figure 10, NH_3 only causes an energy shift of the C1s peak when it is adsorbed on the fluorinated surface. Therefore, when the NH_3 is adsorbed between substrate and FG, it is of course still observed as NH_3 in the XPS spectra, but its binding to the pristine graphene on the backside will not lead to doping effects on graphene. And thus, despite the presence of residual NH_3, no doping effect in C1s is expected as was observed.

The analysis of the F1s peaks in Figure 12 (b) also indicates a shift towards higher binding energies. This shift reflects the doping effect induced by NH_3 across the entire spectrum.

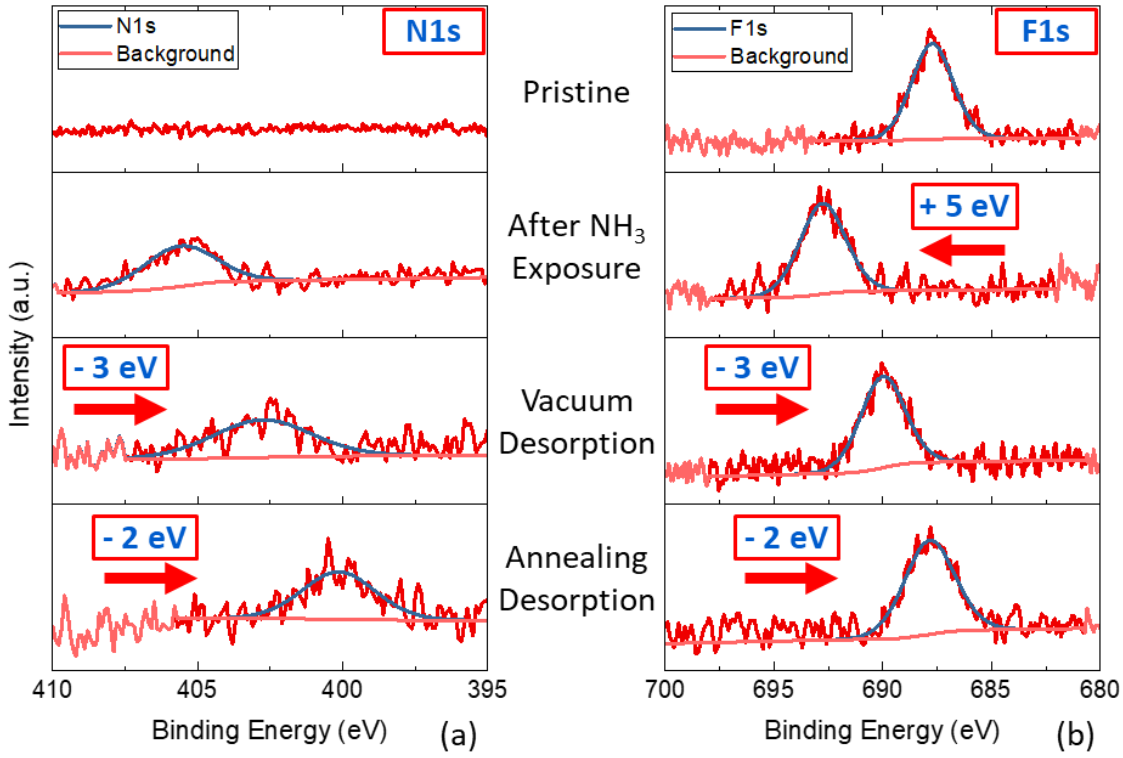

Figure 12. XPS spectra of the N1s (a) and F1s (b) from the fluorinated sample, before and after exposure to 10 mbar of NH_3, after a first step of vacuum desorption and after annealing at 250°C.

These results allow for the assessment that there is no preferential adsorption of NH_3 in the fluorinated zone compared to the pristine zone. This finding suggests that the potentially enhanced sensitivity of the NH_3 gas sensor as observed in other studies does not stem from improved adsorption. However, the peak shift effects indicate that the sensor response might be affected by the modification in the charge transport and the doping effects induced by the gas adsorption in a "transient" process.

5. Discussion

Functionalized graphene sensors, particularly those employing fluorinated graphene (FG), hold promise due to their heightened sensitivity to specific target species such as ammonia. To better comprehend this enhanced sensitivity, it is crucial to address the question: what causes the increased conductivity variations observed during NH_3 exposure of such fluorinated devices with defects, GO, rGO or with pristine FG? Two primary hypotheses emerge: firstly, the potential acceleration of adsorption kinetics, with NH_3 preferentially

adsorbing onto fluorinated graphene compared to pristine graphene like DFT simulation results revealed [40,64], and secondly, the potential enhancement of adsorption energy at FG sites [19,65].

For enhanced comprehension, it is known that the response of a graphene/fluorographene gas sensor can be described by a multi-site Langmuir adsorption-desorption phenomenon model where the conductance could be considered as [42,66–78]:

$$G(t) = G^{eq} - \gamma_1 N_1 \left(\theta_1^{eq} - \theta_1^0\right) e^{-\kappa_1 t} - \gamma_2 N_2 \left(\theta_2^{eq} - \theta_2^0\right) e^{-\kappa_2 t} - \ldots - \gamma_x N_x \left(\theta_x^{eq} - \theta_x^0\right) e^{-\kappa_x t}$$

Equation 1

With the number N of site, the decreasing rate κ, the coverage rate θ and the contribution to the conductance γ proportional to the adsorption energy of the site E_a, and the charge quantity given by the adsorbed molecules ΔQ. In that case, the first hypothesis could lead to changes in the number of sites, the decreasing and coverage rate of the fluorographene. On the contrary, the second assumption would induce new adsorption energy of the fluorographene's site.

It is commonly admitted that fluorination enhances the *p* doping of the graphene thereby heightening its reactivity to reducing gases [40,79,80]. The doping by the fluorine molecule introduces a shift of the Fermi level away from of the valence band, enhancing consequently intensifying conduction variations in FG [81]. Additionally, in the case of fluorinated graphene, the distance between the adsorbed NH_3 and the Carbon atoms is reduced [16].

During our experiments, we did not notice a substantial increase in NH_3 adsorption in the fluorinated area compared to the pristine one. Instead, we demonstrated the *n* doping induced by the NH_3 adsorption leading to a global shift of C1s, F1s, and N1s peaks. This shift is reversible through vacuuming and annealing, leading to the complete desorption of NH_3 from the fluorinated graphene. This indicate a slow desorption rate of NH_3. This is in accordance with the slow kinetic observed during graphene gas sensing experiments wich is a typical limitation with long response times [7,8,82–86].

The residual N1s signal observed at the process's conclusion could be attributed to lingering NH_3 molecules present but not interacting with FG or pristine graphene. Remarkably, identical shifts occur in both pristine and fluorinated areas, that could indicate NH_3's preferential interaction with carbon atoms over fluorine atoms. On the other hand, the identical shifts might also highlight the importance of the defects, or oxides group in the enhanced response observed in the existing sensors.

This study seeks to develop a novel approach to better understand the fluorinated graphene gas sensors heightened sensitivity based on XPS cartography. With this tool it is possible, with the analysis of the chemical shifting, to observe the increased adsorption energy of fluorographene sites for NH_3 and by transivity a new contribution to the conductance from the functionalized sites. Similarly, it will enable the identification preferential adsorption zone with an increased signal of the studied species.

6. Conclusion

In conclusion, the study highlights the potential of e-beam fluorinated graphene as a promising material for gas-sensing applications, particularly in detecting ammonia. The e-fluorographene demonstrates excellent stability and resilience even under harsh thermal conditions up to 450°C, essential for sensor reusability. Similarly, it has been shown that the e-fluorination remains stable over a period of several months.

XPS analysis reveals reversible doping effects induced by NH_3 adsorption, with both pristine and fluorinated graphene areas exhibiting similar shifts in peak positions, suggesting NH_3's preferential interaction with carbon atoms. While no preferential adsorption of NH_3 is observed in the fluorinated zone compared to the pristine zone, there is no increase in the bonding coefficient of gas molecules on fluorinated graphene whereas a better sensitivity of the sensor could be expected precisely by the increase of the electronic affinity of the surface for the target gas [19]. Thus, the enhanced sensitivity to NH_3 of fluorinated graphene gas sensors could be attributed to responses in charge transport and doping effects induced by gas adsorption *i.e.* the adsorption energy of the e-fluorographen. However, there were no noticeable differences in the position of the C1s components between the fluorinated and pristine areas during the gas exposure experiment. This suggests that the e-beam fluorination process may not be effective in enhancing the graphene gas sensor's response to NH_3. Therefore, it is crucial to investigate the role of oxide groups and (or) defects in the graphene lattice in the gas exposure response. Their presence may be necessary to increase the adsorption coefficient or the adsorption energy in fluorographene, which could be key to improving sensor performance. Further experiments are warranted to incorporate the fluorographene into a gas-sensing device and thoroughly investigate its response to NH_3 and also NO_2.

These findings contribute to advancing our understanding of FG in gas sensing technologies and underscore its potential for future applications in environmental monitoring and health safety.

Acknowledgements

The Région Grand Est, the European fond Feder through the 'NanoteraHertz' project and the French National Research Agency (ANR) through the project MIXES (grant ANR-19-CE09-0028) are warmly acknowledged for the financial support. This work was also supported by a grant (ANR-21-

EXES-0012 Mat-Light 4.0) from the French National Research Agency (ANR) on behalf of France 2030.

References

[1] A. Dey, Semiconductor metal oxide gas sensors: A review, Mater. Sci. Eng. B Solid-State Mater. Adv. Technol. **229**, 206 (2018).

[2] G. J. Thompson, D. K. Carder, M. C. Besch, A. Thiruvengadam, and H. K. Kappanna, In-use emissions testing of light-duty diesel vehicles in the United States, 1 (2014).

[3] M. Clairotte, Impact of Fuels and Exhaust Aftertreatment Systems on the Unregulated Emissions from Mopeds , Light and Heavy - Duty Vehicles, Université de Montpellier 2, 2014.

[4] X.-Q. Jiang, X.-D. Mei, and D. Feng, Air pollution and chronic airway diseases: what should people know and do?, J. Thorac. Dis. **8**, (2016).

[5] *Ambient (Outdoor) Air Pollution*, https://www.who.int/news-room/fact-sheets/detail/ambient-(outdoor)-air-quality-and-health.

[6] M. Scardamaglia et al., Operando Investigation of WS_2 Gas Sensors: Simultaneous Ambient Pressure X-ray Photoelectron Spectroscopy and Electrical Characterization in Unveiling Sensing Mechanisms during Toxic Gas Exposure, ACS Sens. **9**, 4079 (2024).

[7] F. Schedin, A. K. Geim, S. V. Morozov, E. W. Hill, P. Blake, M. I. Katsnelson, and K. S. Novoselov, Detection of individual gas molecules adsorbed on graphene, Nat. Mater. **6**, 652 (2007).

[8] A. A. Balandin, S. Rumyantsev, G. Liu, M. S. Shur, and R. A. Potyrailo, *Selective Gas Sensing with a Single Graphene-on-Silicon Transistor*, in *2012 IEEE Silicon Nanoelectronics Workshop (SNW)* (IEEE, 2012), pp. 1–2.

[9] S. Rumyantsev, G. Liu, R. A. Potyrailo, A. A. Balandin, M. S. Shur, and L. Fellow, Selective Sensing of Individual Gases Using Graphene Devices, **13**, 2818 (2013).

[10] T. Wang, D. Huang, Z. Yang, S. Xu, G. He, X. Li, N. Hu, G. Yin, D. He, and L. Zhang, A Review on Graphene-Based Gas/Vapor Sensors with Unique Properties and Potential Applications, Nano-Micro Lett. **8**, 95 (2016).

[11] V. Kumar, K. Vanish, and K. Ki-Hyun, Graphene materials as a superior platform for advanced sensing strategies against gaseous ammonia, J. Mater. Chem. A **6**, 22391 (2018).

[12] R. S. Perala, N. Chandrasekar, R. Balaji, P. S. Alexander, N. Z. N. Humaidi, and M. T. Hwang, A comprehensive review on graphene-based materials: From synthesis to contemporary sensor applications, Mater. Sci. Eng. R Rep. **159**, 100805 (2024).

[13] C. I. L. Justino, A. R. Gomes, A. C. Freitas, A. C. Duarte, and T. A. P. Rocha-Santos, Graphene based sensors and biosensors, TrAC - Trends Anal. Chem. **91**, 53 (2017).

[14] L. Daukiya, M. N. Nair, M. Cranney, F. Vonau, S. Hajjar-Garreau, D. Aubel, and L. Simon, Functionalization of 2D materials by intercalation, Prog. Surf. Sci. **94**, 1 (2019).

[15] H. Ruan et al., In Situ Local Band Engineering of Monolayer Graphene Using Triboelectric Plasma, Small **20**, 2309318 (2024).

[16] K. K. Tadi, S. Pal, and T. N. Narayanan, Fluorographene based Ultrasensitive Ammonia Sensor, Sci. Rep. **6**, 25221 (2016).

[17] D. D. Chronopoulos, A. Bakandritsos, M. Pykal, R. Zbořil, and M. Otyepka, Chemistry, properties, and applications of fluorographene, Appl. Mater. Today **9**, 60 (2017).

[18] H. Li, L. Daukiya, S. Haldar, A. Lindblad, B. Sanyal, O. Eriksson, D. Aubel, S. Hajjar-Garreau, L. Simon, and K. Leifer, Site-selective local fluorination of graphene induced by focused ion beam irradiation, Sci. Rep. **6**, 1 (2016).

[19] Y. H. Kim et al., Chemically fluorinated graphene oxide for room temperature ammonia detection at ppb levels, J. Mater. Chem. A **5**, 19116 (2017).

[20] W. Feng, P. Long, Y. Y. Feng, and Y. Li, Two-dimensional fluorinated graphene: Synthesis, structures, properties and applications, Adv. Sci. **3**, 1 (2016).

[21] M. Herraiz, M. Dubois, N. Batisse, S. Hajjar-Garreau, and L. Simon, Large-scale synthesis of fluorinated graphene by rapid thermal exfoliation of highly fluorinated graphite, Dalton Trans. **47**, 4596 (2018).

[22] M. Dubois et al., Thermal exfoliation of fluorinated graphite, Carbon **77**, 688 (2014).

[23] C. Sun, Y. Feng, Y. Li, C. Qin, Q. Zhang, and W. Feng, Solvothermally exfoliated fluorographene for high-performance lithium primary batteries, Nanoscale **6**, 2634 (2014).

[24] X. Chen, K. Fan, Y. Liu, Y. Li, X. Liu, W. Feng, and X. Wang, Recent Advances in Fluorinated Graphene from Synthesis to Applications: Critical Review on Functional Chemistry and Structure Engineering, Adv. Mater. **34**, 2101665 (2022).

[25] S.-H. Cheng, K. Zou, F. Okino, H. R. Gutierrez, A. Gupta, N. Shen, P. C. Eklund, J. O. Sofo, and J. Zhu, Reversible fluorination of graphene: Evidence of a two-dimensional wide bandgap semiconductor, Phys. Rev. B (2010).

[26] R. R. Nair et al., Fluorographene: A Two-Dimensional Counterpart of Teflon, Small **6**, 2877 (2010).

[27] V. Mazánek, O. Jankovský, J. Luxa, D. Sedmidubský, Z. Janoušek, F. Šembera, M. Mikulics, and Z. Sofer, Tuning of fluorine content in graphene: towards large-scale production of stoichiometric fluorographene, Nanoscale **7**, 13646 (2015).

[28] S. D. Costa, J. E. Weis, O. Frank, Z. Bastl, and M. Kalbac, Thermal treatment of fluorinated graphene: An in situ Raman spectroscopy study, Carbon **84**, 347 (2015).

[29] H. Wang, M. Narasaki, Z. Zhang, K. Takahashi, J. Chen, and X. Zhang, Ultra-strong stability of double-sided fluorinated monolayer graphene and its electrical property characterization, Sci. Rep. **10**, 1 (2020).

[30] R. J. Kashtiban, M. A. Dyson, R. R. Nair, R. Zan, S. L. Wong, Q. Ramasse, A. K. Geim, U. Bangert, and J. Sloan, Atomically resolved imaging of highly ordered alternating fluorinated graphene, Nat. Commun. **5**, (2014).

[31] F. Withers, T. H. Bointon, M. Dubois, S. Russo, and M. F. Craciun, Nanopatterning of fluorinated graphene by electron beam irradiation, Nano Lett. **11**, 3912 (2011).

[32] R. Stine, W. K. Lee, K. E. Whitener, J. T. Robinson, and P. E. Sheehan, Chemical stability of graphene fluoride produced by exposure to XeF 2, Nano Lett. **13**, 4311 (2013).

[33] A. V. Okotrub, I. P. Asanov, N. F. Yudanov, K. S. Babin, A. V. Gusel'nikov, T. I. Nedoseikina, P. N. Gevko, L. G. Bulusheva, Z. Osváth, and L. P. Biró, Development of graphene layers by reduction of graphite fluoride C2F surface, Phys. Status Solidi B Basic Res. **246**, 2545 (2009).

[34] D. W. Boukhvalov, Absence of a stable atomic structure in fluorinated graphene, Phys. Chem. Chem. Phys. **18**, 13287 (2016).

[35] F. Withers, S. Russo, M. Dubois, and M. F. Craciun, Tuning the electronic transport properties of graphene through functionalisation with fluorine, Nanoscale Res. Lett. **6**, 1 (2011).

[36] V. I. Sysoev, M. O. Bulavskiy, D. V. Pinakov, G. N. Chekhova, I. P. Asanov, P. N. Gevko, L. G. Bulusheva, and A. V. Okotrub, Chemiresistive Properties of Imprinted Fluorinated Graphene Films, Materials **13**, 3538 (2020).

[37] H. Barès, A. Bakandritsos, M. Medveď, J. Ugolotti, P. Jakubec, O. Tomanec, S. Kalytchuk, R. Zbořil, and M. Otyepka, Bimodal role of fluorine atoms in fluorographene chemistry opens a simple way toward double functionalization of graphene, Carbon **145**, 251 (2019).

[38] T. N. Narayanan, R. K. Biroju, and V. Renugopalakrishnan, Fluorographene: Synthesis and sensing applications, J. Mater. Res. **32**, 2848 (2017).

[39] X. Tang, M. Debliquy, D. Lahem, Y. Yan, and J.-P. Raskin, A Review on Functionalized Graphene Sensors for Detection of Ammonia, Sensors **21**, 1443 (2021).

[40] H. Zhang, L. Fan, H. Dong, P. Zhang, K. Nie, J. Zhong, Y. Li, J. Guo, and X. Sun, Spectroscopic Investigation of Plasma-Fluorinated Monolayer Graphene and Application for Gas Sensing, ACS Appl. Mater. Interfaces **8**, 8652 (2016).

[41] W. Kang and S. Li, Preparation of fluorinated graphene to study its gas sensitivity, RSC Adv. **8**, 23459 (2018).

[42] T. Duan, H. Li, L. Daukiya, L. Simon, and K. Leifer, Enhanced Ammonia Gas Adsorption through Site-Selective Fluorination of Graphene, Crystals **12**, 1117 (2022).

[43] W. Lai, D. Xu, X. Wang, Z. Wang, Y. Liu, X. Zhang, and X. Liu, Characterizations of the thermal/thermal oxidative stability of fluorinated graphene with various structures, (2017).

[44] T. Chen, Effects of the oxygenic groups on the mechanism of fluorination of graphene oxide and its structure, (2017).

[45] V. Malesys, A. Andrieux-Ledier, P. Lavenus, and L. Simon, Building a cm^2 scale CVD graphene-based gas sensor: modelling the kinetic with a three-

site adsorption/desorption Langmuir model., Nanotechnology (2024).

[46] J. Gu, X. Guo, W. Xia, P. Peng, F. Du, and L. Li, Facile synthesis of fluorinated graphene for surface self-assembly of aluminum hydride, FirePhysChem **3**, 201 (2023).

[47] H. Li, T. Duan, S. Haldar, B. Sanyal, O. Eriksson, H. Jafri, S. Hajjar-Garreau, L. Simon, and K. Leifer, Direct writing of lateral fluorographene nanopatterns with tunable bandgaps and its application in new generation of moiré superlattice, Appl. Phys. Rev. **7**, 011403 (2020).

[48] T. Duan, H. Li, and K. Leifer, Electron-Beam-Induced Fluorination Cycle for Long-Term Preservation of Graphene under Ambient Conditions, Nanomaterials **12**, (2022).

[49] Th. Le Mogne, J.-M. Martin, and C. Grossiord, *Imaging the Chemistry of Transfer Films in the AES/XPS Analytical UHV Tribotester*, in *Tribology Series*, Vol. 36 (Elsevier, 1999), pp. 413–421.

[50] C. Zhang et al., Multielement Activity Mapping and Potential Mapping in Solid Oxide Electrochemical Cells through the use of *operando* XPS, ACS Catal. **2**, 2297 (2012).

[51] R. Ghobeira, P. S. Esbah Tabaei, R. Morent, and N. De Geyter, Chemical characterization of plasma-activated polymeric surfaces via XPS analyses: A review, Surf. Interfaces **31**, 102087 (2022).

[52] X. Liang et al., Toward Clean and Crackless Transfer of Graphene, ACS Nano **5**, 9144 (2011).

[53] J. T. Robinson et al., Properties of fluorinated graphene films, Nano Lett. **10**, 3001 (2010).

[54] X. Wang, Y. Dai, J. Gao, J. Huang, B. Li, C. Fan, J. Yang, and X. Liu, High-Yield Production of Highly Fluorinated Graphene by Direct Heating Fluorination of Graphene-oxide, ACS Appl. Mater. Interfaces **5**, 8294 (2013).

[55] X. Wang, W. Wang, D. Xu, Y. Liu, W. Lai, and X. Liu, Activation effect of porous structure on fluorination of graphene based materials with large specific surface area at mild condition, Carbon **124**, 288 (2017).

[56] B. Zhou, X. Qian, M. Li, J. Ma, L. Liu, C. Hu, Z. Xu, and X. Jiao, Tailoring the chemical composition and dispersion behavior of fluorinated graphene oxide via CF4 plasma, J. Nanoparticle Res. **17**, 130 (2015).

[57] B. Wang, J. Wang, and J. Zhu, Fluorination of Graphene: A Spectroscopic and Microscopic Study, ACS Nano **8**, 1862 (2014).

[58] C. Sun, Y. Feng, Y. Li, C. Qin, Q. Zhang, and W. Feng, Solvothermally exfoliated fluorographene for high- performance lithium primary batteries, (2014).

[59] X. Wang, S. Liu, H. Han, X. Liu, and X. Wang, Research progress in insulating and thermal conductivity of fluorinated graphene and its polyimide composites, IET Nanodielectrics nde2.12068 (2023).

[60] A. Tressaud, F. Moguet, S. Flandrois, M. Chambon, C. Guimon, G. Nanse, E. Papirer, V. Gupta, and O. P. Bahl, On the nature of C□F bonds in various fluorinated carbon materials: XPS and TEM investigations, J. Phys. Chem. Solids **57**, 745 (1996).

[61] L. T. Zhuravlev, The surface chemistry of amorphous silica. Zhuravlev model, Colloids Surf. Physicochem. Eng. Asp. **173**, 1 (2000).

[62] P. Blake et al., Graphene-Based Liquid Crystal Device, Nano Lett. **8**, 1704 (2008).

[63] X. Wang, L. Zhi, and K. Müllen, Transparent, Conductive Graphene Electrodes for Dye-Sensitized Solar Cells, Nano Lett. **8**, 323 (2008).

[64] T. Wu, Q. Xue, C. Ling, M. Shan, Z. Liu, Y. Tao, and X. Li, Fluorine-Modified Porous Graphene as Membrane for CO2/N2 Separation: Molecular Dynamic and First-Principles Simulations, J Phys Chem C (2014).

[65] Y. Liu, The naked-eye NH3 sensor based on fluorinated graphene, (2018).

[66] I. Langmuir, THE ADSORPTION OF GASES ON PLANE SURFACES OF GLASS, MICA AND PLATINUM., J. Am. Chem. Soc. **40**, 1361 (1918).

[67] W. Wongwiriyapan et al., Single-walled carbon nanotube thin-film sensor for ultrasensitive gas detection, Jpn. J. Appl. Phys. Part 2 Lett. **44**, (2005).

[68] I. H. Wani, S. H. M. Jafri, J. Warna, A. Hayat, H. Li, V. A. Shukla, A. Orthaber, A. Grigoriev, R. Ahuja, and K. Leifer, A sub 20 nm metal-conjugated molecule junction acting as a nitrogen dioxide sensor, Nanoscale **11**, 6571 (2019).

[69] Y. Battie, O. Ducloux, P. Thobois, N. Dorval, J. S. Lauret, B. Attal-Trétout, and A. Loiseau, Gas sensors based on thick films of semi-conducting

single walled carbon nanotubes, Carbon **49**, 3544 (2011).
[70] W. Wongwiriyapan, S. Inoue, S. ichi Honda, and M. Katayama, Adsorption kinetics of NO2 on single-walled carbon nanotube thin-film sensor, Jpn. J. Appl. Phys. **47**, 8145 (2008).
[71] C. Wen, Q. Ye, S. L. Zhang, and D. Wu, Assessing kinetics of surface adsorption-desorption of gas molecules via electrical measurements, Sens. Actuators B Chem. **223**, 791 (2016).
[72] C. Mackin, V. Schroeder, A. Zurutuza, C. Su, J. Kong, T. M. Swager, and T. Palacios, Chemiresistive Graphene Sensors for Ammonia Detection, ACS Appl. Mater. Interfaces **10**, 16169 (2018).
[73] S. Yang, C. Jiang, and S. huai Wei, Gas sensing in 2D materials, Appl. Phys. Rev. **4**, (2017).
[74] S.-Z. Liang, G. Chen, A. R. Harutyunyan, M. W. Cole, and J. O. Sofo, Analysis and optimization of carbon nanotubes and graphene sensors based on adsorption-desorption kinetics, Appl. Phys. Lett. **103**, 233108 (2013).
[75] M. Gautam and A. H. Jayatissa, Graphene based field effect transistor for the detection of ammonia, J. Appl. Phys. **112**, (2012).
[76] M. Gautam and A. H. Jayatissa, Adsorption kinetics of ammonia sensing by graphene films decorated with platinum nanoparticles, J. Appl. Phys. **111**, 094317 (2012).
[77] M. Gautam and A. H. Jayatissa, Ammonia gas sensing behavior of graphene surface decorated with gold nanoparticles, Solid-State Electron. **78**, 159 (2012).
[78] S. Angizi, E. Y. C. Yu, J. Dalmieda, D. Saha, P. R. Selvaganapathy, and P. Kruse, Defect Engineering of Graphene to Modulate pH Response of Graphene Devices, Langmuir **37**, 12163 (2021).
[79] Y. Zhang, Y. Chen, K. Zhou, C. Liu, J. Zeng, H.-L. Zhang, and Y. Peng, Improving gas sensing properties of graphene by introducing dopants and defects: a first-principles study, Nanotechnology **20**, 185504 (2009).
[80] Z. Zhang, X. X. Zhang, W. Luo, H. Yang, Y. He, Y. Liu, X. X. Zhang, and G. Peng, Study on adsorption and desorption of ammonia on graphene, Nanoscale Res. Lett. **10**, (2015).
[81] M. Park, K. H. Kim, M. Kim, and Y. Lee, NH 3 gas sensing properties of a gas sensor based on fluorinated graphene oxide, Colloids Surf. Physicochem. Eng. Asp. **490**, 104 (2016).
[82] S. Novikov, N. Lebedeva, and A. Satrapinski, Ultrasensitive NO 2 Gas Sensor Based on Epitaxial Graphene, J. Sens. **2015**, 1 (2015).
[83] R. Pearce, T. Iakimov, M. Andersson, L. Hultman, A. L. Spetz, and R. Yakimova, Epitaxially grown graphene based gas sensors for ultra sensitive NO 2 detection, Sens. Actuators B Chem. **155**, 451 (2011).
[84] G. Lu, L. E. Ocola, and J. Chen, Gas detection using low-temperature reduced graphene oxide sheets, Appl. Phys. Lett. **94**, 083111 (2009).
[85] G. Chen, T. M. Paronyan, and A. R. Harutyunyan, Sub-ppt gas detection with pristine graphene, Appl. Phys. Lett. **101**, 053119 (2012).
[86] F. Yavari, E. Castillo, H. Gullapalli, P. M. Ajayan, and N. Koratkar, High sensitivity detection of NO 2 and NH 3 in air using chemical vapor deposition grown graphene, Appl. Phys. Lett. **100**, (2012).